Chapter 3

Compact stars on pseudo-spheroidal spacetime compatible with observational data

In this chapter, we have studied two models of anisotropic fluid distributions on the background of a pseudo-spheroidal spacetime by assuming two different pressure distributions. The physical acceptability of the models are investigated and found that they are compatible with a number of pulsars of known mass and size.

3.1 Introduction

The study of compact objects in agreement with observational data has received wide attention among researchers. A number of superdense star models compatible with observational data, have appeared in literature in the recent past (Murad

[2013a], Murad [2013b], Murad and Fatema [2013, 2015a], Pandya et al. [2015], Gangopadhyay et al. [2013], Hansraj and Maharaj [2006], Tikekar and Jotania [2009], Banerjee et al. [2013], Maurya et al. [2017b], Sharma and Ratanpal [2013]). If spacetime admitting compact star models possess a definite three-space geometry, then it is a mathematically interesting problem also. The spheroidal spacetimes studied by Vaidya and Tikekar [1982], Tikekar [1990], Tikekar and Thomas [1998], Thomas et al. [2005], Thomas and Ratanpal [2007], Tikekar and Jotania [2005], and Chattopadhyay and Paul [2010] and the paraboloidal spacetime studied by Finch and Skea [1989], Tikekar and Jotania [2007], Sharma and Ratanpal [2013] and Pandya et al. [2015] are examples of spacetimes with definite 3-space geometry. The superdense star models developed by Tikekar and Thomas [1998] has pseudo-spheroidal geometry. A number of researchers used this spacetime for developing physically viable models of compact stars under different assumptions on the physical content.

Theoretical investigations of Ruderman [1972] and Canuto [1974] suggest that matter may not isotropic in ultra high density regime. After the publication of the work of Bowers and Liang [1974], there has been a large number of models devoted to the study of anisotropic distribution of matter. Maharaj and Maartens [1989] developed an anisotropic model with uniform density and Gokhroo and Mehra [1994] gave a more realistic anisotropic model with non-uniform density. Tikekar and Thomas [1999, 2005], Thomas et al. [2005] developed superdense anisotropic distributions on pseudo-spheroidal spacetimes. Thomas and Ratanpal [2007] studied non-adiabatic gravitational collapse of anisotropic distribution of matter accompanied by radial heat flux. Dev and Gleiser [2002, 2003, 2004] have studied the impact of anisotropy on the stability of stellar configuration. Anisotropic distributions of matter incorporating linear equation of state have been studied by Sharma and Maharaj [2007], & Thirukkanesh and Maharaj [2008]. Komathiraj and Maharaj [2007a] have stud-

ied charged distribution using linear equation of state. Sunzu et al. [2014] studied charged anisotropic quark stars using linear equation of state. Anisotropic distributions of matter incorporating quadratic equation of state have been given by Feroze and Siddiqui [2011] & Maharaj and Takisa [2012]. Varela et al. [2010] used linear and non-linear equations of state for describing charged anisotropic distributions of matter. Paul et al. [2011] have shown, in the MIT bag model of quark stars, that anisotropy can affect the bag constant. Polytropic equations of state has been used by Thirukkanesh and Ragel [2012] & Maharaj and Takisa [2013]. Malaver [2013a,b, 2014] and Thirukkanesh and Ragel [2014] have used modified Van der Waals equation of state for describing anisotropic charged compact stars.

In 2015, Pandya et al. [2015] have developed anisotropic models of compact stars compatible with observational data by generalizing Finch and Skea [1989] ansatz. The anisotropic stellar model given by Sharma and Ratanpal [2013] is a subclass of the model of Pandya et al. [2015].

This model accommodates the observational data of a variety of compact objects recently studied by researchers. In the present chapter, we have obtained a new class of anisotropic stellar model of compact objects on the background of pseudo-spheroidal spacetime. The physical parameter p_0 and geometric parameter K appearing in the model are restricted as a result of various physical acceptability conditions imposed on the model. Another geometric parameter R of the model plays the role of the radius of the spherical distribution of matter. It is found that our model yields values of different physical quantities that are in good agreement with the most recently available observational data of compact objects (Gangopadhyay et al. [2013]) like 4U 1820-30, PSR J1903+327, 4U 1608-52, Vela X-1, PSR J1614-2230, SMC X-4 and

Cen X-3.

3.2 Spacetime metric

We take the interior metric describing the anisotropic matter distribution in the form

$$ds^2 = e^{\nu(r)}dt^2 - \frac{1+K\frac{r^2}{R^2}}{1+\frac{r^2}{R^2}}dr^2 - r^2d\theta^2 - r^2sin^2\theta d\phi^2, \tag{3.1}$$

where, K, R are geometric parameters and $K > 1$. This spacetime, generally known as pseudo-spheroidal spacetime, has been studied by many researchers (Tikekar and Thomas [1998, 1999, 2005], Thomas et al. [2005], Thomas and Ratanpal [2007], Paul et al. [2011], Chattopadhyay and Paul [2010], Chattopadhyay et al. [2012]).

Following Maharaj and Maartens [1989], we write the energy-momentum tensor for anisotropic matter distribution in the form

$$T_{ij} = (\rho + p)\, u_i u_j - p g_{ij} + \pi_{ij}, \tag{3.2}$$

where, ρ, p and u_i denote the proper density, fluid pressure and unit four-velocity of the fluid, respectively.

The anisotropic stress-tensor π_{ij} is given by

$$\pi_{ij} = \sqrt{3}S\left[C_iC_j - \frac{1}{3}(u_iu_j - g_{ij})\right], \tag{3.3}$$

where, $C^i = (0, -e^{-\lambda/2}, 0, 0)$ is a radial vector and $S = S(r)$ denotes the magnitude of the anisotropic stress.

The non-vanishing components of the energy-momentum tensor are given by

$$T_0^0 = \rho, \quad T_1^1 = -\left(p + \frac{2S}{\sqrt{3}}\right), \quad T_2^2 = T_3^3 = -\left(p - \frac{S}{\sqrt{3}}\right). \tag{3.4}$$

Hence the radial and transverse pressures are given by

$$p_r = -T_1^1 = \left(p + \frac{2S}{\sqrt{3}}\right), \tag{3.5}$$

$$p_\perp = -T_2^2 = \left(p - \frac{S}{\sqrt{3}}\right). \tag{3.6}$$

Then the magnitude of the anisotropic stress has the form

$$S = \frac{p_r - p_\perp}{\sqrt{3}}. \tag{3.7}$$

The physical and geometric variables, related through Einstein's field equations

$$R_{ij} - \frac{1}{2}Rg_{ij} = 8\pi T_{ij}, \tag{3.8}$$

are to be determined from the following set of three equations:

$$8\pi\rho = \frac{1 - e^{-\lambda}}{r^2} + \frac{e^{-\lambda}\lambda'}{r}, \tag{3.9}$$

$$8\pi p_r = \frac{e^{-\lambda} - 1}{r^2} - \frac{e^{-\lambda}\nu'}{r}, \tag{3.10}$$

$$8\pi p_\perp = e^{-\lambda}\left[\frac{\nu''}{2} + \frac{\nu'^2}{4} - \frac{\nu'\lambda'}{4} + \frac{\nu' - \lambda'}{2r}\right], \tag{3.11}$$

where a prime denotes a differentiation with respect to r. The equations (3.9) – (3.11) can be couched in the form

$$e^{-\lambda} = 1 - \frac{2m}{r}, \tag{3.12}$$

$$\left(1 - \frac{2m}{r}\right)\nu' = 8\pi p_r r + \frac{2m}{r^2}, \tag{3.13}$$

$$-\frac{4}{r}(8\pi\sqrt{3}S) = (8\pi\rho + 8\pi p_r)\nu' + 2(8\pi p_r'), \tag{3.14}$$

where

$$m(r) = 4\pi \int_0^r u^2 \rho(u) du. \tag{3.15}$$

The energy-density ρ and the mass m within the radius r have expressions

$$8\pi\rho = \frac{K-1}{R^2} \frac{\left(3 + K\frac{r^2}{R^2}\right)}{\left(1 + K\frac{r^2}{R^2}\right)^2}, \tag{3.16}$$

$$m(r) = \frac{R}{2} \frac{(K-1)\frac{r^2}{R^2}}{1 + \frac{Kr^2}{R^2}}. \tag{3.17}$$

It can be easily obtained from equation (3.12) that

$$8\pi\rho' = -\frac{2K(K-1)r}{R^4} \frac{\left(5 + K\frac{r^2}{R^2}\right)}{\left(1 + K\frac{r^2}{R^2}\right)^3} < 0, \tag{3.18}$$

indicating that the density decreases radially outward.

3.3 Anisotropic Model 1

In order to obtain the metric potential ν, we assume an expression for p_r in equation (3.13), in the form

$$8\pi p_r = \frac{p_0}{R^2} \frac{\left(1 - \frac{r^2}{R^2}\right)\left(1 + \frac{r^2}{R^2}\right)}{\left(1 + K\frac{r^2}{R^2}\right)^2}. \tag{3.19}$$

The radial pressure in the present form vanishes at $r = R$ and takes the value $\frac{p_0}{R^2}$ at the centre $r = 0$. It is non-negative for all values of r in the range $0 \leq r \leq R$. Further, on differentiating equation (3.19) with respect to r, we get

$$8\pi p_r' = -\frac{4p_0 r\left(K + \frac{r^2}{R^2}\right)}{R^4\left(1 + K\frac{r^2}{R^2}\right)^3} < 0, \tag{3.20}$$

indicating that the pressure p_r decreases radially outward. Since $p_r(r = R) = 0$, the geometric parameter R takes the role of the boundary radius of the distribution. With this choice of p_r, equation (3.13) can be integrated to obtain ν in the form

$$e^{\nu} = A\left(1 + K\frac{r^2}{R^2}\right)^{\frac{p_0(K+1)}{2K^2}}\left(1 + \frac{r^2}{R^2}\right)^{\frac{K-1}{2}} exp\left\{\frac{-p_0}{2K^2}\left(1 + K\frac{r^2}{R^2}\right)\right\} \tag{3.21}$$

where A is a constant of integration.

Therefore, the spacetime metric takes the explicit form

$$ds^2 = A\left(1 + K\frac{r^2}{R^2}\right)^{\frac{p_0(K+1)}{2K^2}}\left(1 + \frac{r^2}{R^2}\right)^{\frac{K-1}{2}} \times exp\left\{\frac{-p_0}{2K^2}\left(1 + K\frac{r^2}{R^2}\right)\right\}dt^2 - \frac{1 + K\frac{r^2}{R^2}}{1 + \frac{r^2}{R^2}}dr^2 - r^2d\theta^2 - r^2sin^2\theta d\phi^2. \tag{3.22}$$

The constant of integration A can be obtained by matching the interior spacetime metric (3.1) with the Schwarzschild exterior metric

$$ds^2 = \left(1 - \frac{2m}{r}\right)dt^2 - \left(1 - \frac{2m}{r}\right)^{-1}dr^2 - r^2d\theta^2 - r^2sin^2\theta d\phi^2 \tag{3.23}$$

across the boundary $r = R$. This gives

$$R = \frac{2M(K+1)}{(K-1)}, \tag{3.24}$$

and

$$A = \frac{2}{K+1}\left(\frac{e}{K+1}\right)^{\frac{(K+1)p_0}{2K^2}} 2^{-\left(\frac{K-1}{2}\right)}. \tag{3.25}$$

The expression for anisotropy is now readily available by substituting for p_r, p_r' and ν' in the equation (3.14).

$$8\pi\sqrt{3}S = \frac{r^2}{R^2}\left(\frac{2p_0\left(K+\frac{r^2}{R^2}\right)}{R^2\left(1+\frac{Kr^2}{R^2}\right)^3} - \frac{B(r)C(r)}{R^2\left(1+K\frac{r^2}{R^2}\right)}\right), \tag{3.26}$$

where

$$B(r) = \left[\frac{p_0\left(1-\frac{r^2}{R^2}\right)}{4\left(1+\frac{Kr^2}{R^2}\right)^4} + \frac{K-1}{4\left(1+\frac{r^2}{R^2}\right)}\right], \tag{3.27}$$

$$C(r) = \left[(K-1)\left(3+K\frac{r^2}{R^2}\right) + p_0\left(1-\frac{r^4}{R^4}\right)\right]. \tag{3.28}$$

It is easy to see that S vanishes at origin $r = 0$, which is a desired requirement for anisotropic distributions (Murad [2013a], Murad [2013b], Murad and Fatema [2013, 2015a] & Bowers and Liang [1974]).

The expression for transverse pressure

$$8\pi p_\perp = 8\pi p_r - 8\pi\sqrt{3}S \tag{3.29}$$

can be obtained using equations (3.19) and (3.26).

Moreover, the condition $p_\perp \geq 0$ will lead to the following inequality at $r = R$

$$p_0 \leq \frac{1}{16}(K-1)^2(K+3), \tag{3.30}$$

whereas at $r = 0$, the condition is evidently satisfied.

The expressions for $\frac{dp_r}{d\rho}$ and $\frac{dp_\perp}{d\rho}$ are given by

$$\frac{dp_r}{d\rho} = \frac{2p_0}{K(K-1)}\frac{\left(K+\frac{r^2}{R^2}\right)}{\left(5+K\frac{r^2}{R^2}\right)}, \tag{3.31}$$

$$\frac{dp_\perp}{d\rho} = \frac{dp_r}{d\rho} - \sqrt{3}\frac{dS}{d\rho}. \tag{3.32}$$

The conditions $0 \leq \frac{dp_r}{d\rho} \leq 1$ and $0 \leq \frac{dp_\perp}{d\rho} \leq 1$ at $r = 0$, respectively, give the inequalities

$$0 \leq p_0 \leq \frac{5}{2}(K-1), \tag{3.33}$$

and

$$0 \leq p_0 \leq \frac{K(K-1)(K+5)}{2(K+1)}. \tag{3.34}$$

Similarly the above conditions at $r = R$, respectively, give

$$2(3K+1) - \sqrt{33K^2+30K+1} \leq p_0 \leq 2(3K+1) - \sqrt{13K^2+50K+1}, \tag{3.35}$$

and

$$0 < p_0 \leq \frac{-K^4+12K^3+78K^2-92K+3}{8K^2-24K+80}. \tag{3.36}$$

The adiabatic index

$$\Gamma = \frac{\rho + p_r}{p_r}\frac{dp_r}{d\rho} \tag{3.37}$$

has the explicit expression

$$\Gamma = \frac{2\left(K+\frac{r^2}{R^2}\right)C(r)}{K(K-1)\left(5+K\frac{r^2}{R^2}\right)\left(1-\frac{r^4}{R^4}\right)}. \tag{3.38}$$

The necessary condition for the model to represent a relativistic star is that $\Gamma > \frac{4}{3}$ throughout the star. $\Gamma > \frac{4}{3}$ at $r = 0$ impose a condition on p_0, viz.,

$$p_0 > \frac{K-1}{3}. \tag{3.39}$$

The strong energy condition $\rho - p_r - 2p_\perp \geq 0$ at $r = 0$ and $r = R$, respectively, give the following two inequalities

$$p_0 \leq K - 1 \tag{3.40}$$

and

$$p_0 \geq \frac{(K+3)(K-1)(K-5)}{16}. \tag{3.41}$$

In order to obtain a valid range for the parameters p_0 and K, we have to consider the inequalities (3.33) – (3.36) and (3.38) – (3.41) simultaneously.

3.4 Bounds for Model Parameters

The pseudo-spheroidal space-time model developed for anisotropic matter distribution contains a physical parameter p_0 related to the central pressure and two geometric parameters, viz., R and K. Since $p_r(r = R) = 0$, the free parameter R represents the radius of the distribution. The bounds for the other two parameters p_0 and K are to be determined by the following requirements a physically acceptable model is expected to satisfy in its region of validity $0 \leq r \leq R$.

Table 3.1: Bounds for p_0.

Physical requirements	**at** $r = 0$	**at** $r = R$
$\rho - p_r - 2p_\perp \geq 0$	$p_0 \leq K - 1$	$p_0 \geq \frac{(K+3)(K-1)(K-5)}{16}$
$0 \leq \frac{dp_r}{d\rho} \leq 1$	$0 \leq p_0 \leq \frac{5}{2}(K-1)$	$2(3K+1) - \sqrt{(33K^2+30K+1)} \leq p_0$ $\leq 2(3K+1) - \sqrt{(13K^2+50K+1)}$
$0 \leq \frac{dp_\perp}{d\rho} \leq 1$	$0 \leq p_0 \leq \frac{K(K-1)(K+5)}{2(K+1)}$	$0 \leq p_0 \leq \frac{-K^4+12K^3+78K^2-92K+3}{8K^2-24K+80}$
$\Gamma(r) \geq \frac{4}{3}$	$p_0 > \frac{K-1}{3}$	Automatically satisfied

(1) $\rho(r) \geq 0, p_r(r) \geq 0, p_\perp(r) \geq 0$,

(2) $\rho(r) - p_r(r) - 2p_\perp(r) \geq 0$,

(3) $\frac{d\rho(r)}{dr} < 0, \frac{dp_r(r)}{dr} < 0$,

(4) $0 \leq \frac{dp_r}{d\rho} \leq 1, 0 \leq \frac{dp_\perp}{d\rho} \leq 1$,

(5) The adiabatic index $\Gamma(r) > \frac{4}{3}$.

The conditions $\rho(r) \geq 0, p_r(r) \geq 0, \frac{d\rho(r)}{dr} < 0, \frac{dp_r(r)}{dr} < 0$ are automatically satisfied by equations (3.16), (3.19), (3.18), (3.20).

We have displayed in Table 3.1 the bounds on p_0 in terms of the parameter K at the centre and on the boundary.

We have displayed the numerical values of the lower and upper bounds of p_0 for different values of $K > 1$ in Table 3.2. We have considered the maximum of all lower limits of p_0 and minimum of all its upper limits. The admissible values of K are those for which minimum of upper limit minus maximum of lower limit is positive. This condition restricts the values of K in the range $(2.05, 5.69)$. It is further observed that for $2.05 < K \leq 3.47, 3.47 \leq K \leq 5.24$, and $5.24 \leq K < 5.69, p_0$ satisfies, respectively, the inequalities $\frac{K-1}{3} < p_0 \leq \frac{(K+3)(K-1)^2}{16}, \frac{K-1}{3} \leq p_0 \leq K - 1$ and

Table 3.2: Permissible values of K and p_0.

$LP1 = \frac{K-1}{3}$,
$LP2 = \frac{(K+3)(K-1)(K-5)}{6}$,
$LP3 = 2(3K+1) - \sqrt{(33K^2+30K+1)}$,
$UP1 = \frac{(K+3)(K-1)^2}{16}$,
$UP2 = K-1$,
$UP3 = \frac{5(K-1)}{2}$,
$UP4 = \frac{K(K-1)(K+5)}{2(K+1)}$,
$UP5 = 2(3K+1) - \sqrt{(13K^2+50K+1)}$,
$UP6 = \frac{-K^4+12K^3+78K^2-92K+3}{8K^2-24K+80}$.

K	**Lower Limit for p_0**			**Max**	**Upper Limit for p_0**						**Min**	**Min - Max**
	$LP1$	$LP2$	$LP3$		$UP1$	$UP2$	$UP3$	$UP4$	$UP5$	$UP6$		
2	**0.33**	-2.50	0.11	**0.33**	**0.31**	1	2.5	2.33	1.63	3.30	**0.31**	-0.02
2.05	**0.35**	-2.61	0.12	**0.35**	**0.35**	1.05	2.625	2.49	1.72	3.54	**0.35**	**0.00**
2.1	**0.37**	-2.71	0.12	**0.37**	**0.39**	1.1	2.75	2.65	1.82	3.78	**0.39**	0.02
2.4	**0.47**	-3.28	0.18	**0.47**	**0.66**	1.4	3.5	3.66	2.40	5.32	**0.66**	0.19
2.8	**0.60**	-3.83	0.26	**0.60**	**1.17**	1.8	4.5	5.17	3.21	7.40	**1.17**	0.57
3	**0.67**	-4.00	0.30	**0.67**	**1.50**	2	5	6.00	3.63	8.40	**1.50**	0.83
3.1	**0.70**	-4.06	0.32	**0.70**	**1.68**	2.1	5.25	6.43	3.84	8.88	**1.68**	**0.98**
3.2	**0.73**	-4.09	0.35	**0.73**	**1.88**	2.2	5.5	6.87	4.05	9.35	**1.88**	1.14
3.4	**0.80**	-4.10	0.39	**0.80**	**2.30**	2.4	6	7.79	4.48	10.23	**2.30**	1.50
3.47	**0.82**	-4.08	0.40	**0.82**	**2.47**	2.47	6.175	8.12	4.63	10.53	**2.47**	**1.64**
3.8	**0.93**	-3.81	0.48	**0.93**	3.33	**2.8**	7	9.75	5.34	11.79	**2.80**	1.87
4	**1.00**	-3.50	0.52	**1.00**	3.94	**3**	7.5	10.80	5.78	12.46	**3.00**	2.00
4.2	**1.07**	-3.07	0.57	**1.07**	4.61	**3.2**	8	11.89	6.22	13.05	**3.20**	2.13
4.4	**1.13**	-2.52	0.62	**1.13**	5.35	**3.4**	8.5	13.02	6.66	13.58	**3.40**	2.27
4.8	**1.27**	-0.99	0.71	**1.27**	7.04	**3.8**	9.5	15.41	7.55	14.45	**3.80**	2.53
5	**1.33**	0.00	0.76	**1.33**	8.00	**4**	10	16.67	8.00	14.80	**4.00**	2.67
5.2	**1.40**	1.15	0.81	**1.40**	9.04	**4.2**	10.5	17.97	8.45	15.10	**4.20**	2.80
5.24	**1.41**	1.40	0.82	**1.41**	9.26	**4.24**	10.6	18.23	8.54	15.15	**4.24**	**2.83**
5.4	1.47	**2.46**	0.85	**2.46**	10.16	**4.4**	11	19.31	8.90	15.35	**4.40**	1.94
5.67	1.56	**4.52**	0.92	**4.52**	11.82	**4.67**	11.675	21.18	9.52	15.63	**4.67**	0.15
5.69	1.56	**4.69**	0.92	**4.69**	11.95	**4.69**	11.725	21.32	9.56	15.64	**4.69**	**0.00**
5.71	1.57	**4.85**	0.93	**4.85**	12.08	**4.71**	11.775	21.46	9.61	15.66	**4.71**	-0.14

$\frac{1}{6}(K+3)(K-1)(K-5) \leq p_0 < K-1$. The shaded region in Figure 3.1 gives the permissible values of K and p_0. Any values of K and p_0 outside this region may violate one or other of the physical requirements of the model.

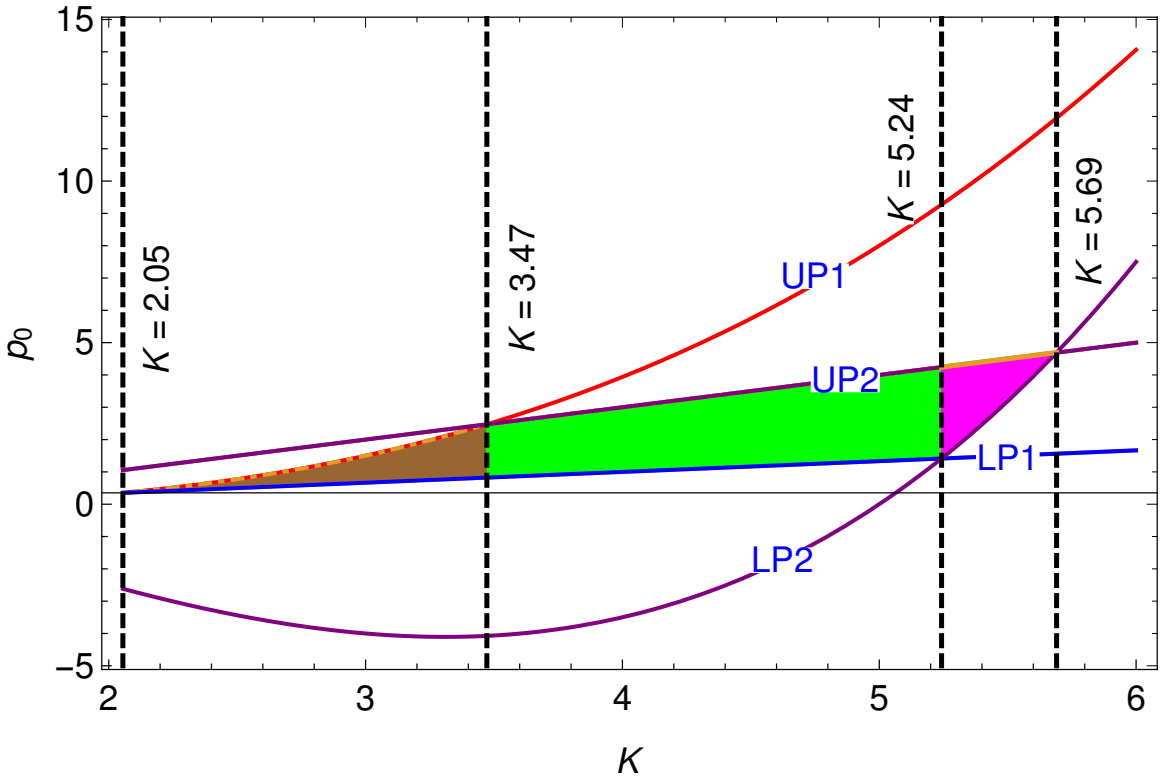

Figure 3.1: Permissible values of p_0 and K.

3.5 Compact Star Models

In order to validate the model, we examine our model with observational data. We have considered the pulsar 4U 1820-30 whose estimated mass and radius are $1.58M_{\odot}$ and 9.1 km (Gangopadhyay et al. [2013]). If we set these values for mass and radius then from equation (3.24) we obtain the value of $K = 3.1$ which is well inside the valid range for K. Similarly assuming masses of some well studied compact stars like PSR J1903+327, 4U 1608-52, Vela X-1, PSR J1614-2230, SMC X-4 and Cen X-3, we have obtained the same radius calculated by Gangopadhyay et al. [2013] for values of K in the valid range. The values of mass, radius, K and other relevant quantities like central density ρ_c, density at the boundary ρ_R, the compactification parameter u and $\frac{dp_r}{d\rho}$ at the centre for $p_0 = 1.08$, are shown in Table 3.3.

Table 3.3: Estimation of physical values based on observational data for $p_0 = 1.08$.

STAR	K	M ($M_\odot$)	R (Km)	ρ_c (MeV fm^{-3})	ρ_R (MeV fm^{-3})	$u(=\frac{M}{R})$	$\left(\frac{dp_r}{d\rho}\right)_{r=0}$
4U 1820-30	3.100	1.58	9.1	2290.97	277.12	0.256	0.206
PSR J1903+327	3.176	1.667	9.438	2129.82	257.62	0.261	0.199
4U 1608-52	3.458	1.74	9.31	2188.78	267.75	0.276	0.176
Vela X-1	3.407	1.77	9.56	2075.80	251.08	0.273	0.179
PSR J1614-2230	3.997	1.97	9.69	2020.48	244.39	0.300	0.144
SMC X-4	2.514	1.29	8.831	2432.67	294.25	0.215	0.285
Cen X-3	2.838	1.49	9.178	2252.20	272.42	0.239	0.235

In order to examine the nature of various physical quantities throughout the distribution, we have considered a particular star 4U 1820-30 for which mass $M = 1.58M_\odot$, radius $R = 9.1km$, the physical parameter $p_0 = 1.08$ and the geometric parameter $K = 3.1$. We have shown the variation of density and pressures in Figure 3.2 and Figure 3.3, respectively. It is observed that the transverse pressure $p_\perp$ is less than the radial pressure for r in the range $0 < r < 2.78903$. Subsequently $p_\perp$ dominates p_r in the region $2.78903 < r \leq 9.1$. The radial pressure p_r vanishes at $r = 9.1$. In Figure 3.4, we have shown the variation of anisotropy throughout the distribution. The variations of sound speed in the radial and transverse directions are shown in Figure 3.5. From Figure 3.6, it is evident that the strong energy condition, $\rho - p_r - 2p_\perp \geq 0$ is satisfied throughout the distribution. Though we have not assumed any explicit expression for the EOS in our model, we have shown the nature of variation of pressures p_r and $p_\perp$ against density in Figure 3.7. For a relativistic model to be stable in its region of validity, we must have the adiabatic index $\Gamma > \frac{4}{3}$. The variation Γ against radius is shown in Figure 3.8. It is clear from Figure 3.8 that $\Gamma > \frac{4}{3}$ throughout the star. The variation of gravitational red shift, $z(r) = \sqrt{e^{-\nu(r)}} - 1$ in the radial direction is shown in Figure 3.9. It is easy to note that the red shift is monotonically decreasing function from the centre to boundary. Further, the red shift at the centre z_c and on the boundary z_R are both positive and finite.

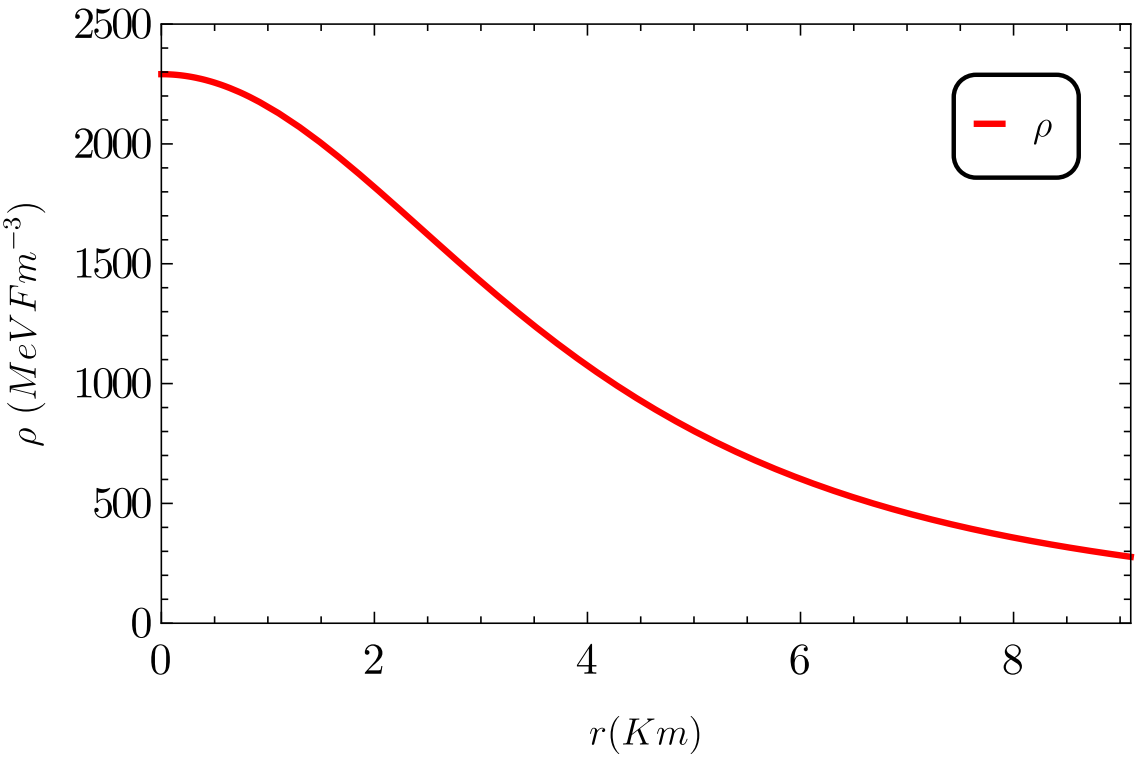

Figure 3.2: Density Vs Radius

3.6 Discussion

Spherical distribution of matter on pseudo-spheroidal spacetimes have been studied by a number of researchers in the recent past Tikekar and Thomas [1998, 1999, 2005], Thomas et al. [2005], Thomas and Ratanpal [2007], Paul et al. [2011], Chattopadhyay and Paul [2010], Chattopadhyay et al. [2012]. In this chapter, we have obtained a new class of solutions to Einstein's field equations for a spherically symmetric anisotropic distribution of matter and have shown that our model can fit to the observational data of a number of well studied pulsars (Gangopadhyay et al. [2013]). On assuming a particular form of radial pressure and on the basis of elementary criteria for physical acceptability of a compact spherically symmetric distribution of matter, we have obtained the bounds for the physical as well as geometric parameters of the model. It is found that our model can accommodate a number of pulsars

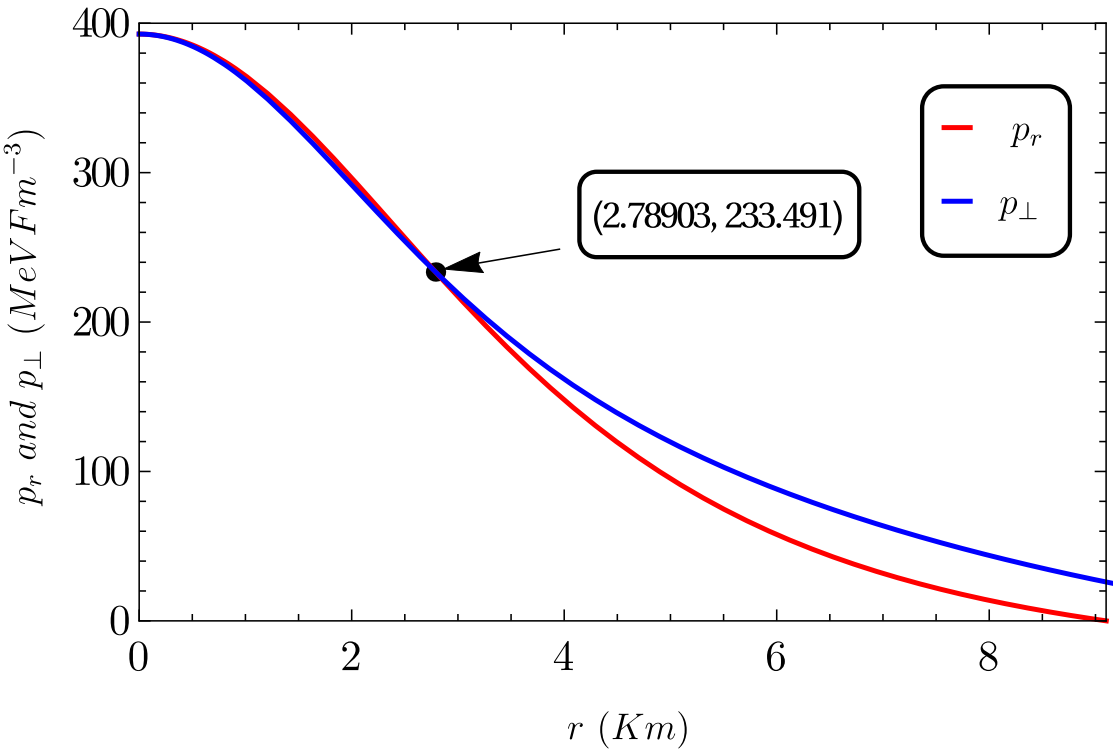

Figure 3.3: Radial and Transverse Pressures Vs Radius

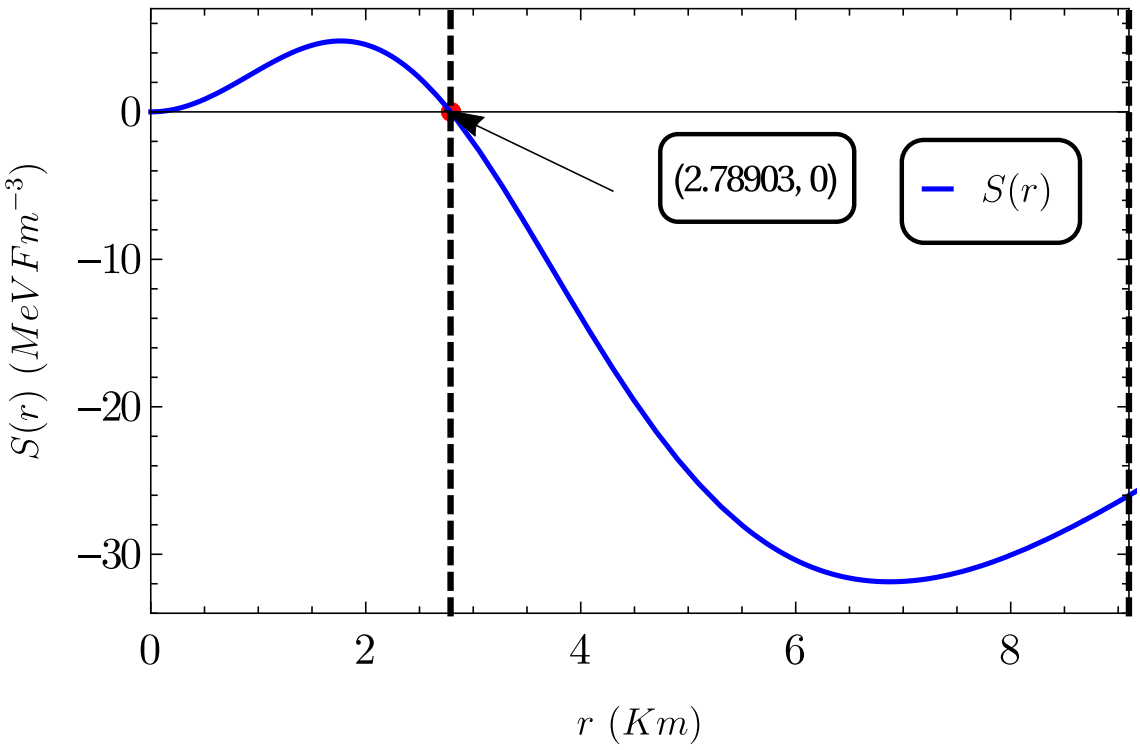

Figure 3.4: Anisotropy Vs Radius

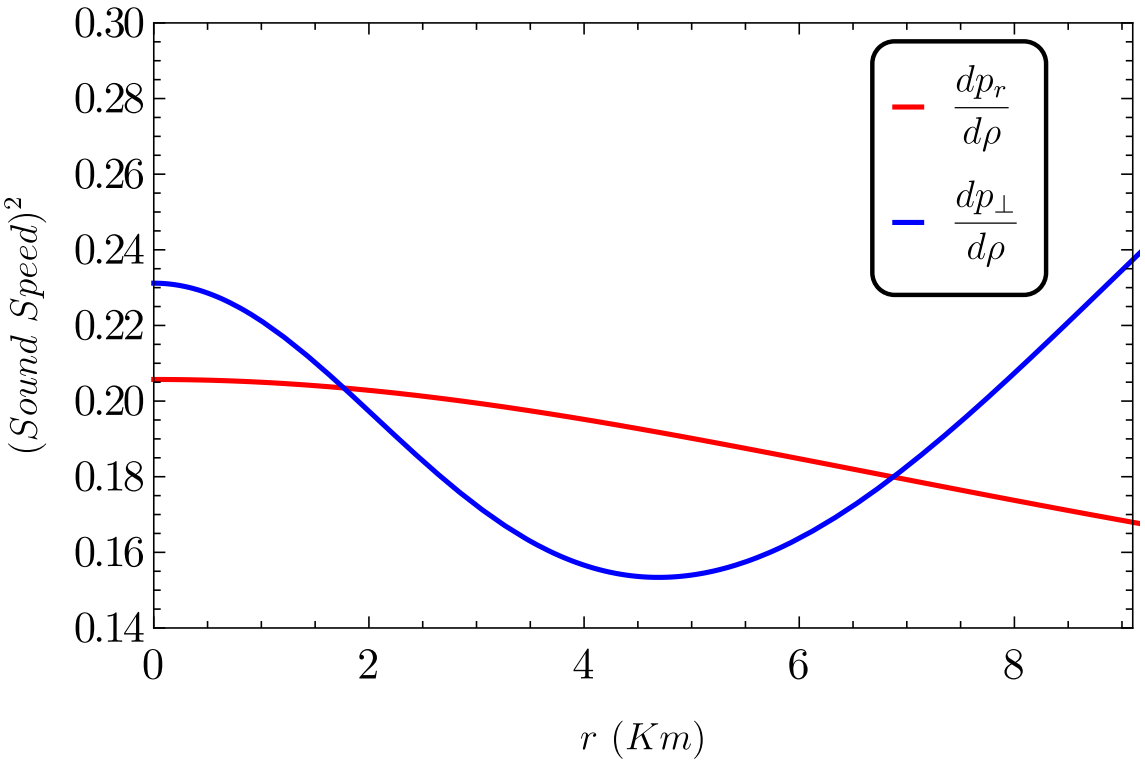

Figure 3.5: $(SoundSpeed)^2$ Vs Radius

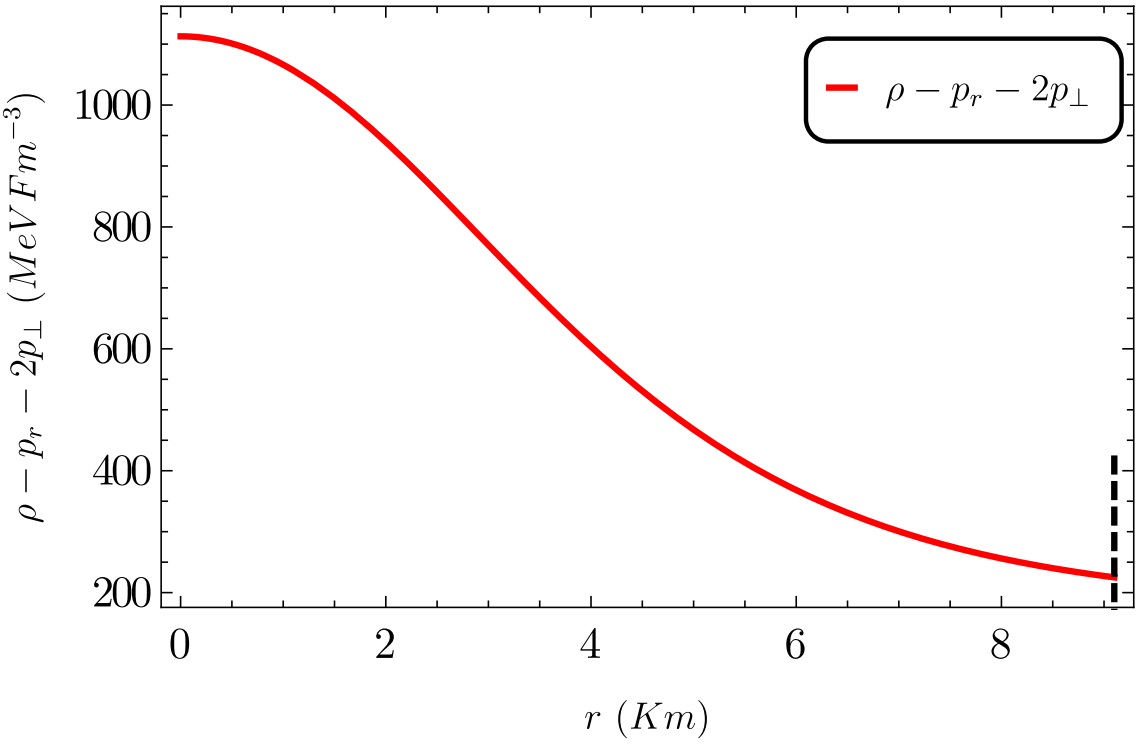

Figure 3.6: Strong Energy Condition Vs Radius

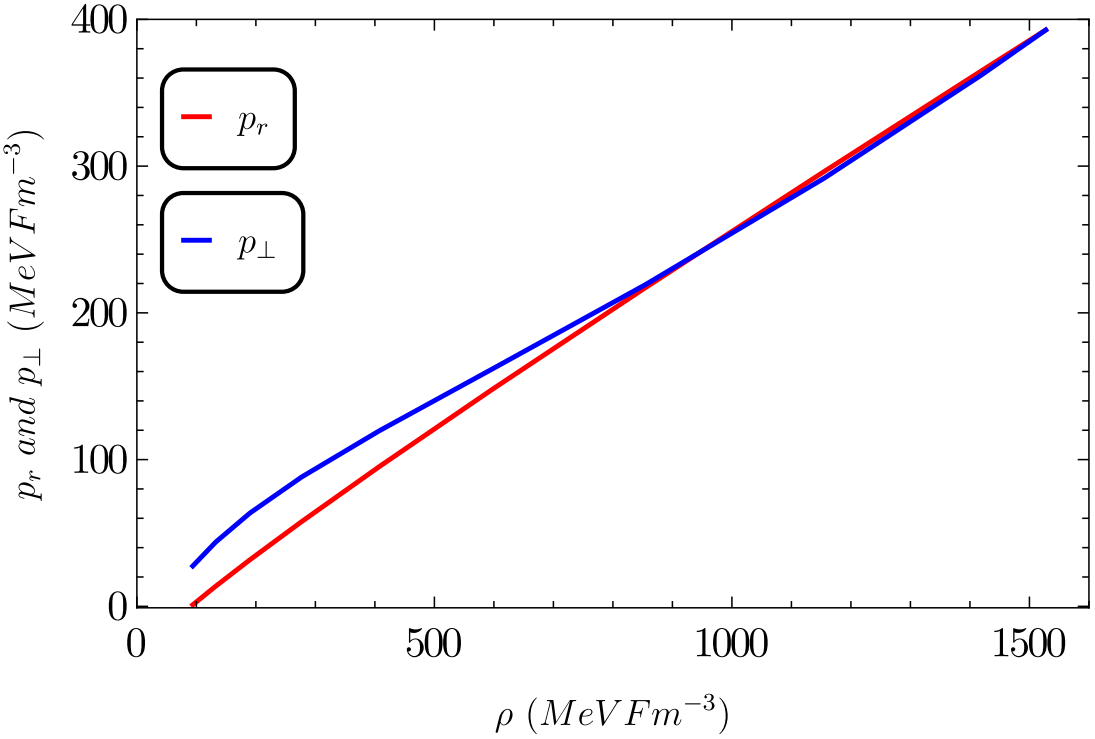

Figure 3.7: Equation of State

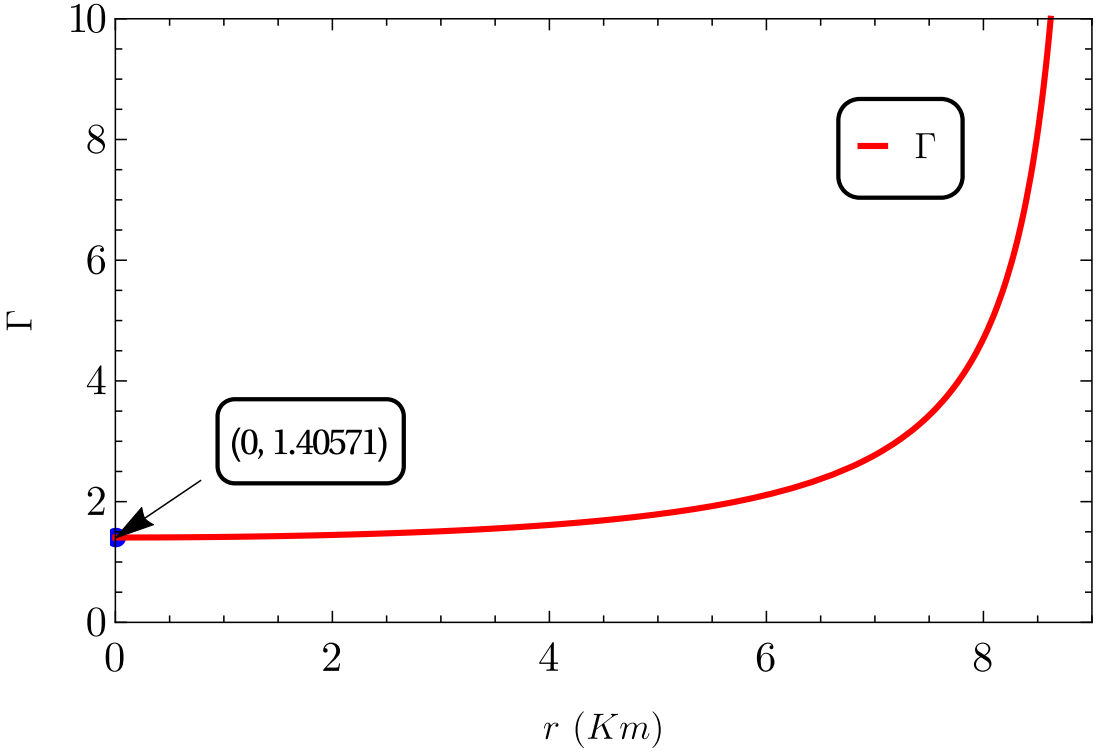

Figure 3.8: Adiabatic Index Vs Radius

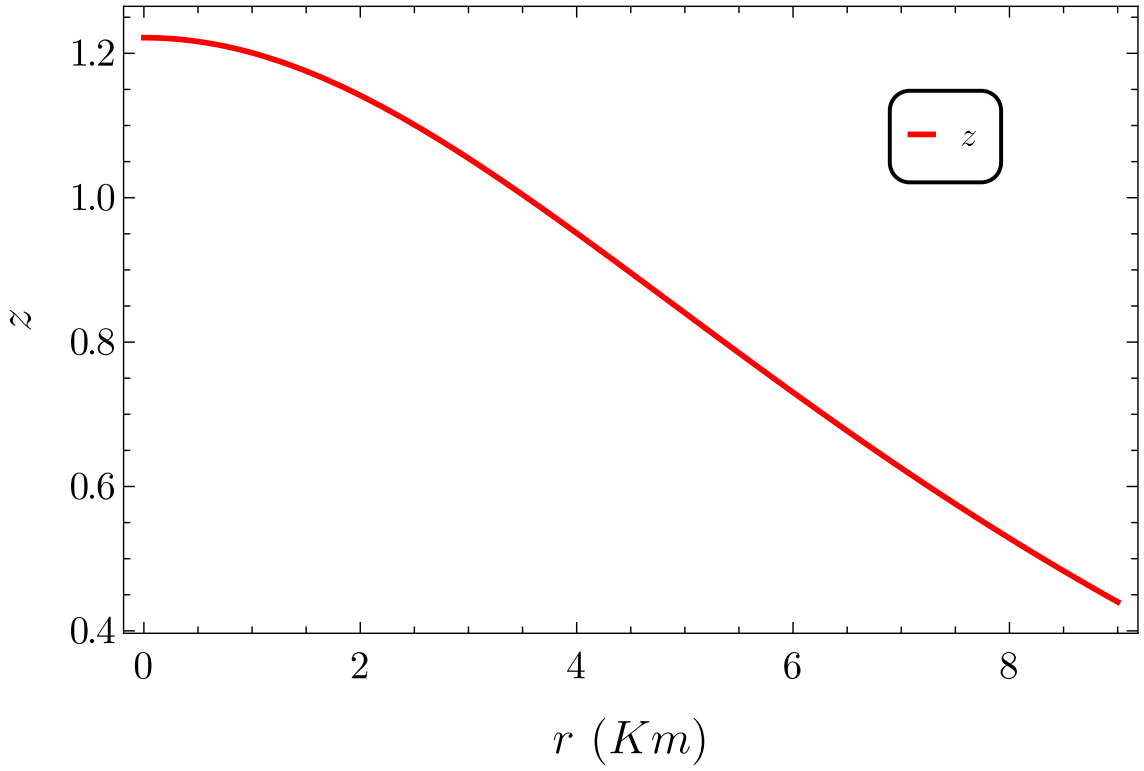

Figure 3.9: Gravitational Red Shift

like 4U 1820-30, PSR J1903+327, 4U 1608-52, Vela X-1, PSR J1614-2230, SMC X-4 and Cen X-3. We also have studied, in detail, a particular pulsar 4U 1820-30, and have shown graphically the profile of different physical quantities throughout the distribution. In short, study of compact stars on the background of pseudo-spheroidal spacetime is highly interesting in the sense that it generates models compatible with observational data and at the same time having a definite 3-space geometry, namely, pseudo-spheroidal geometry which many other spacetimes may not possess.

3.7 Anisotropic Model 2

In this model, in order to obtain the metric potential ν from equation (3.13), we shall take the expression for radial pressure p_r as

$$8\pi p_r = \frac{K-1}{R^2}\frac{1-\frac{r^2}{R^2}}{\left(1+K\frac{r^2}{R^2}\right)^2}. \tag{3.42}$$

It can be noticed from equation (3.42) that the central pressure is $p_r(0) = \frac{K-1}{R^2}$, which is directly related to the geometric parameters K and R. This choice of p_r facilitate the integration of equation (3.13) and obtain e^{ν} in the form

$$e^{\nu} = CR^{\frac{K^2-2K+1}{K}}\left(1+K\frac{r^2}{R^2}\right)^{\frac{K+1}{2K}}\left(1+\frac{r^2}{R^2}\right)^{\frac{K-3}{2}}, \tag{3.43}$$

where C is a constant of integration.

Differentiating equation (3.42) with respect to r, we get

$$8\pi\frac{dp_r}{dr} = -\frac{2r(K-1)}{R^4}\frac{1+K\left(2-\frac{r^2}{R^2}\right)}{\left(1+K\frac{r^2}{R^2}\right)^3}. \tag{3.44}$$

It can be noticed from equation (3.44) that

$$8\pi\frac{dp_r}{dr}(r=0) = 0, \tag{3.45}$$

$$8\pi\frac{dp_r}{dr}(r=R) = -\frac{2(K-1)}{R^2(1+K)^2} < 0. \tag{3.46}$$

Further $8\pi\frac{dp_r}{dr} < 0$ for all values of r in the range $0 \leq r \leq R$. Hence the radial pressure is decreasing radially outward and becomes zero at $r = R$, which is taken as the radius of the anisotropic fluid distribution.

The spacetime metric (3.1) now takes the explicit form

$$\begin{aligned} ds^2 &= CR^{\frac{K^2-2K+1}{K}}\left(1+K\frac{r^2}{R^2}\right)^{\frac{K+1}{2K}}\left(1+\frac{r^2}{R^2}\right)^{\frac{K-3}{2}}dt^2-\left(\frac{1+K\frac{r^2}{R^2}}{1+\frac{r^2}{R^2}}\right)dr^2 \\ &\quad -r^2\left(d\theta^2+\sin^2\theta d\phi^2\right). \end{aligned} \tag{3.47}$$

For a physically acceptable relativistic distribution of matter, the interior spacetime metric (3.47) should continuously match with Schwarzschild exterior metric

$$ds^2=\left(1-\frac{2M}{r}\right)dt^2-\left(1-\frac{2M}{r}\right)^{-1}dr^2-r^2\left(d\theta^2+\sin^2\theta d\phi^2\right), \tag{3.48}$$

across the boundary $r=R$. This gives the constants M and C as

$$M=\frac{R}{2}\frac{(K-1)}{(K+1)}, \tag{3.49}$$

and

$$C=R^{-\left(\frac{K^2-2K+1}{K}\right)}(1+K)^{-\left(\frac{3K+1}{2K}\right)}2^{\left(\frac{5-K}{2}\right)}. \tag{3.50}$$

The expression for anisotropy S can be obtained using (3.16), (3.42), (3.43) and (3.44) in (3.14). We have

$$8\pi\sqrt{3}S=\frac{(K-1)r^2\left[12+\left(-6K^2+16K-2\right)\frac{r^2}{R^2}+\left(-K^3+3K^2-7K+1\right)\frac{r^2}{R^2}\right]}{4R^4\left(1+K\frac{r^2}{R^2}\right)^3\left(1+\frac{r^2}{R^2}\right)}, \tag{3.51}$$

which takes the value zero at $r=0$. The expression for $8\pi p_\perp=8\pi p_r-8\pi\sqrt{3}S$, now takes the form

$$8\pi p_\perp=\frac{(K-1)\left[4+(4K-12)\frac{r^2}{R^2}+\left(6K^2-16K-2\right)\frac{r^4}{R^4}+\left(K^3-3K^2+3K-1\right)\frac{r^6}{R^6}\right]}{4R^2\left(1+K\frac{r^2}{R^2}\right)^3\left(1+\frac{r^2}{R^2}\right)}, \tag{3.52}$$

3.8 Physical Analysis

The anisotropic matter distribution described on the background of pseudo-spheroidal spacetime contains two geometric parameters R and K. Since $p_r(r = R) = 0$, the parameter R represents the radius of the distribution. The bounds on the other parameter K is to be determined using the physical plausibility conditions stipulated below:

(i) $\rho(r),\ p_r(r),\ p_\perp(r) \geq 0$ for $0 \leq r \leq R$;

(ii) $\rho - p_r - 2p_\perp \geq 0$ for $0 \leq r \leq R$;

(iii) $\frac{d\rho}{dr},\ \frac{dp_r}{dr},\ \frac{dp_t}{dr} < 0$ for $0 \leq r \leq R$;

(iv) $0 \leq \frac{dp_r}{d\rho} \leq 1$; $0 \leq \frac{dp_\perp}{d\rho} \leq 1$, for $0 \leq r \leq R$;

(v) The adiabatic index $\Gamma(r) > \frac{4}{3}$, for $0 \leq r \leq R$.

The conditions $\rho(r) \geq 0$, $p_r \geq 0$, $\frac{d\rho}{dr} < 0$ and $\frac{dp_r}{dr} < 0$ are evidently satisfied in the light of equations (3.16), (3.42), (3.18), and (3.46), respectively.

The condition $p_\perp > 0$ imposes a restriction on the value of K, namely,

$$K \geq 2.4641. \tag{3.53}$$

In order to examine the strong energy condition, we evaluate the expression $\rho - p_r - 2p_\perp$ at $r = 0$ and at $r = R$. It is easy to see that

$$(\rho - p_r - 2p_\perp)\,(r = 0) = 0, \tag{3.54}$$

and $(\rho - p_r - 2p_\perp)\,(r = R) \geq 0$, imposes an upper bound for K, namely,

$$K \leq 4.1231. \tag{3.55}$$

It has been suggested by Canuto [1974] that the velocity of sound should be monotonically decreasing for matter distribution with ultra-high densities. This demands that $\frac{d}{dr}\left(\frac{dp_r}{d\rho}\right) < 0$.

The expressions for $\frac{dp_r}{d\rho}$ and $\frac{dp_\perp}{d\rho}$ are, respectively, given by

$$\frac{dp_r}{d\rho} = \frac{1+2K-K\frac{r^2}{R^2}}{K\left(5+K\frac{r^2}{R^2}\right)}, \tag{3.56}$$

$$\frac{dp_\perp}{d\rho} = \frac{\left(1+K\frac{r^2}{R^2}\right)^3\left[X_1+X_2\frac{r^2}{R^2}+X_3\frac{r^4}{R^4}+X_4\frac{r^6}{R^6}+X_5\frac{r^8}{R^8}\right]}{2K(K-1)\left(5+K\frac{r^2}{R^2}\right)\left[2+Y_1\frac{r^2}{R^2}+Y_2\frac{r^4}{R^4}+Y_3\frac{r^6}{R^6}+Y_4\frac{r^8}{R^8}+Y_5\frac{r^{10}}{R^{10}}+2K^4\frac{r^{12}}{R^{12}}\right]}, \tag{3.57}$$

where, $X_1 = 8K^2+8K-16$, $X_2 = -4K^3+28K^2-20K-4$, $X_3 = 3K^4-4K^3-30K^2+36K-5$, $X_4 = 10K^4-36K^3+16K^2+12K-2$, $X_5 = K^5-4K^4+6K^3-4K^2+4$ and $Y_1 = 8K+4$, $Y_2 = 12K^2+16K+2$, $Y_3 = 8K^3+24K^2+8K$, $Y_4 = 2K^4+16K^3+12K^2$, $Y_5 = 4K^4+8K^3$.

It can be noticed from (3.56) that $\frac{dp_r}{d\rho} \leq 1$ throughout the distribution.

The condition $\frac{dp_\perp}{d\rho} \leq 1$ at $r = 0$ and $r = R$ gives the following bounds on K, viz.,

$$K > 1.3333, \tag{3.58}$$

and

$$1 \leq K \leq 14.7882. \tag{3.59}$$

The expression for adiabatic index Γ is given by

$$\Gamma = \frac{\left(4-\frac{r^2}{R^2}+K\frac{r^2}{R^2}\right)\left(1+2K-K\frac{r^2}{R^2}\right)}{K\left(1-\frac{r^2}{R^2}\right)\left(5+K\frac{r^2}{R^2}\right)}. \tag{3.60}$$

The necessary condition for the model to represent a relativistic star is that $\Gamma > \frac{4}{3}$

throughout the star. $\Gamma > \frac{4}{3}$ at $r = 0$ imposes a condition on K, viz.,

$$K > -3. \tag{3.61}$$

Considering all the relevant inequalities, we find that the admissible bound for K is given by

$$2.4641 \leq K \leq 4.1231. \tag{3.62}$$

3.9 Application to Compact Stars and Discussion

In order to examine the suitability of our model to fit into the observational data, we have considered the masses and radii of some well known pulsars given by Gangopadhyay et al. [2013]. We have considered PSR J1614-2230 whose estimated mass and radius are $1.97M_{\odot}$ and 9.69 km. If we set these values in equation (3.49) we get $K = 3.997$ which is well inside the valid range of K. We have further verified that our model is in good agreement with the estimated mass and radii of a number of compact stars like Vela X-1, 4U1608-52, PSRJ1903+327, 4U1820-30 SMC X-4 and Cen X-3. The value of K, mass, radius and other relevant quantities like ρ_c, ρ_R, $u = \frac{M}{R}$ and $\frac{dp_r}{d\rho}(r = 0)$ are shown in Table 3.4.

Table 3.4: Estimated physical values based on the observational data

STAR	K	M ($M_{\odot}$)	R (Km)	ρ_c (MeV fm^{-3})	ρ_R (MeV fm^{-3})	$u(=\frac{M}{R})$	$\left(\frac{dp_r}{d\rho}\right)_{r=0}$
4U 1820-30	3.100	1.58	9.1	2290.97	277.12	0.256	0.465
PSR J1903+327	3.176	1.667	9.438	2206.89	260.52	0.261	0.463
4U 1608-52	3.458	1.74	9.31	2561.92	277.50	0.276	0.458
Vela X-1	3.407	1.77	9.56	2379.27	261.63	0.273	0.459
PSR J1614-2230	**3.997**	**1.97**	**9.69**	**2883.52**	**269.33**	**0.300**	**0.450**
SMC X-4	2.514	1.29	8.831	1753.84	261.06	0.215	0.480
Cen X-3	2.838	1.49	9.178	1971.21	260.42	0.239	0.470

In order to have detailed analysis of various physical conditions throughout the star we have considered a particular star PSR J1614-2230 having mass $M = 1.97M_{\odot}$ and radius $R = 9.69\ km$ along with the geometric parameter $K = 3.997$. The variation of density and pressure from centre to the boundary of the star is shown graphically in Figure 3.10 and Figure 3.11, respectively. It can be seen that density and pressures are monotonically decreasing functions of the radial variable r. In Figure 3.12, we have shown the variation of anisotropy S throughout the star. The anisotropy increases initially and after reaching a maximum at $r = 2.54$, it starts decreasing till the boundary of the star. The variation of square of sound speed and strong energy condition are displayed in Figure 3.13 and Figure 3.14, respectively. It can be noticed that the square of sound speed is less than 1 and the strong energy condition is satisfied throughout the star.

In Figure 3.15, we have shown the equation of state for matter distribution in graphical form. For a stable relativistic star, the adiabatic index Γ should be greater than $\frac{4}{3}$ throughout the configuration. We have plotted the graph of Γ against r in Figure 3.16. The graph clearly indicates that $\Gamma > \frac{4}{3}$ throughout the star. For a physically acceptable model, the gravitational redshift, $z = \sqrt{e^{-\nu(r)}} - 1$, should be a decreasing function of r. Further the central redshift z_c and boundary redshift z_R should be positive and finite. From Figure 3.17, it can be seen that these conditions are satisfied throughout the star.

We have studied spherically symmetric anisotropic distributions of matter on pseudo-spheroidal spacetime. The model we have developed is in good agreement with the observational data of pulsars recently studied by Gangopadhyay et al. [2013]. The model parameters are carefully selected so that the models satisfy all the physical requirements throughout the distribution. We have studied a particular model of PSR J1614-2230 and have shown that various physical requirements stipulated

earlier are satisfied throughout the star.

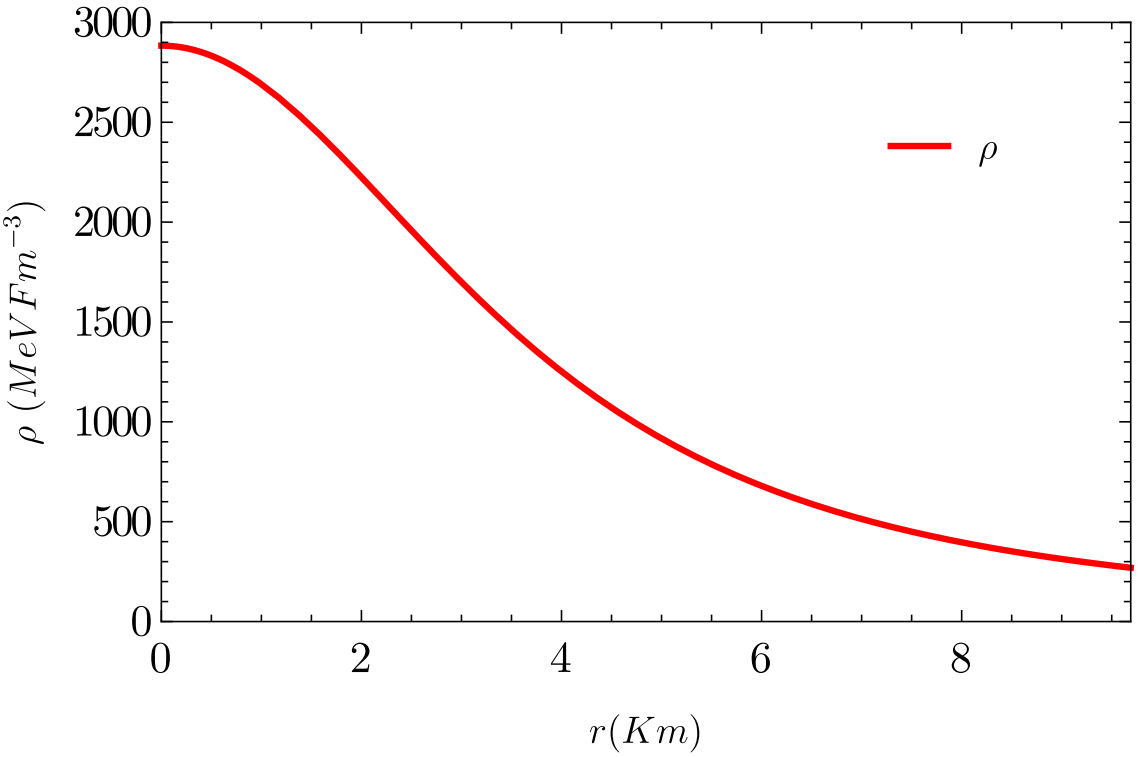

Figure 3.10: Variation of density against radial variable r.

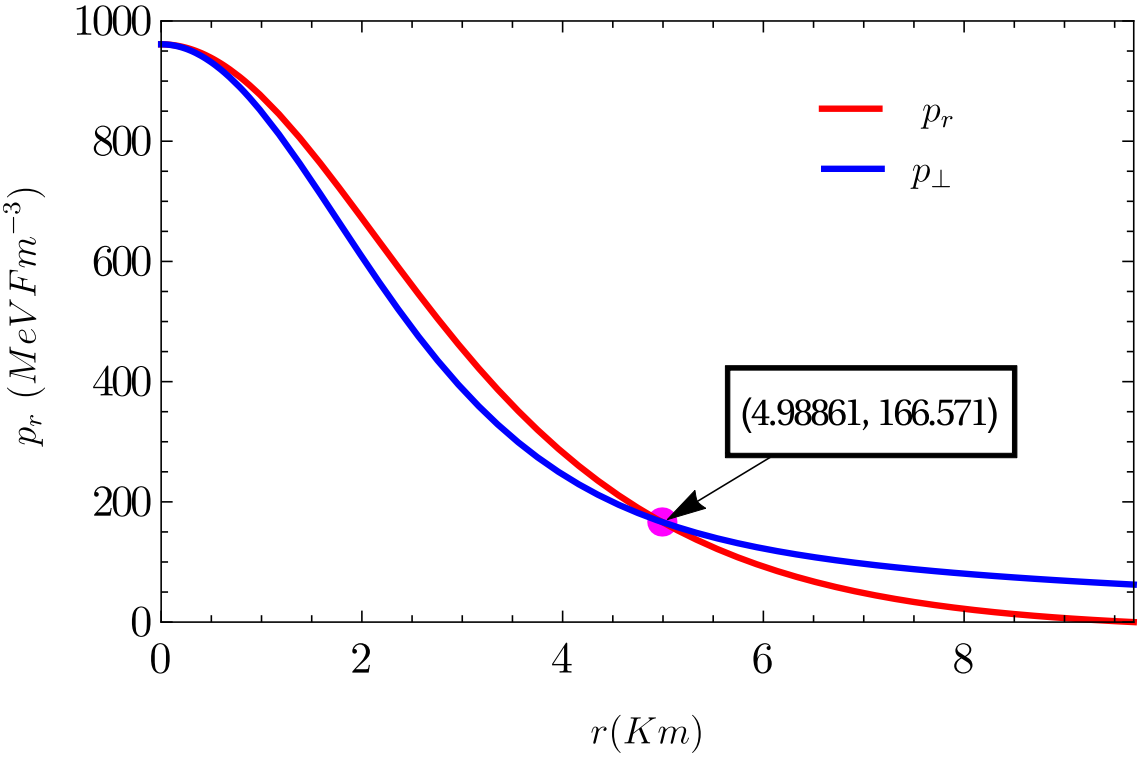

Figure 3.11: Variation of pressures against radial variable r.

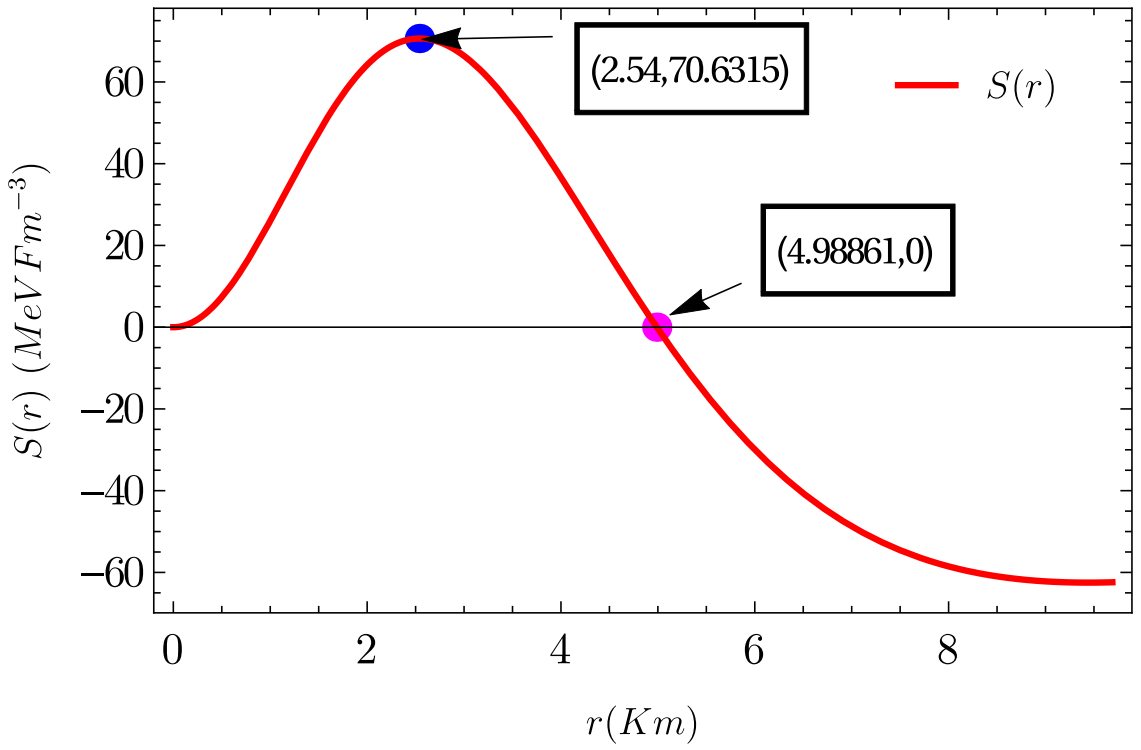

Figure 3.12: Variation of anisotropy against radial variable r.

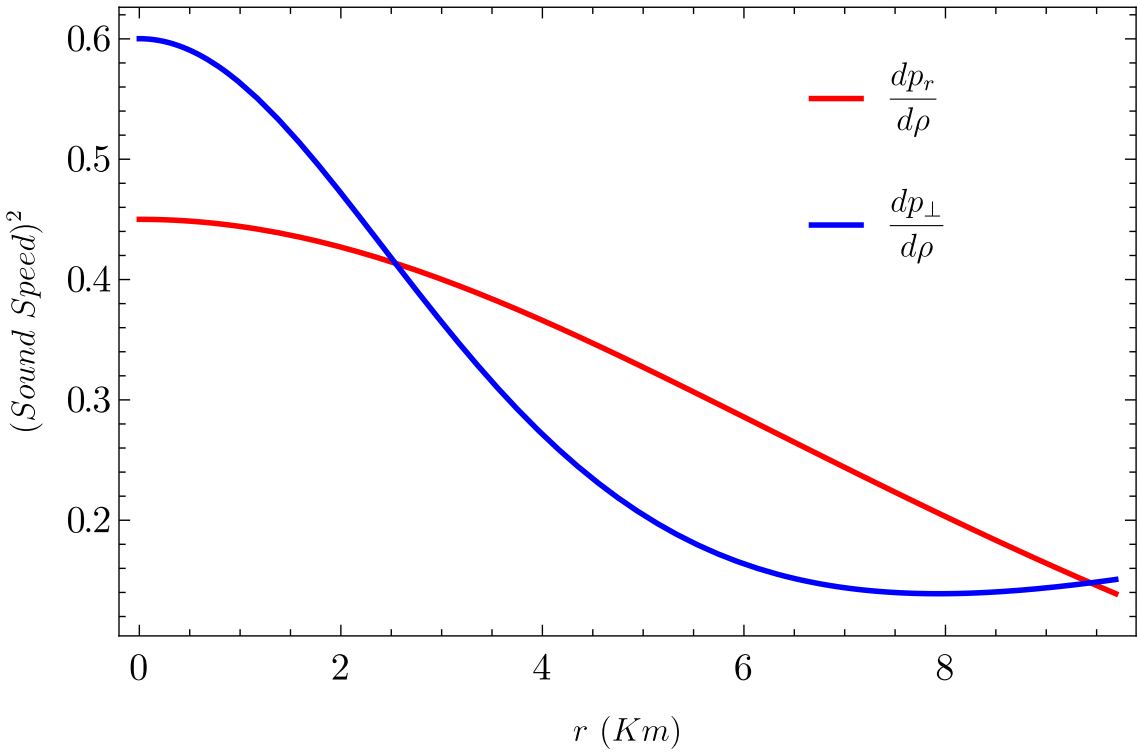

Figure 3.13: Variation of $\frac{1}{c^2}\frac{dp_r}{d\rho}$, $\frac{1}{c^2}\frac{dp_\perp}{d\rho}$ against radial variable r.

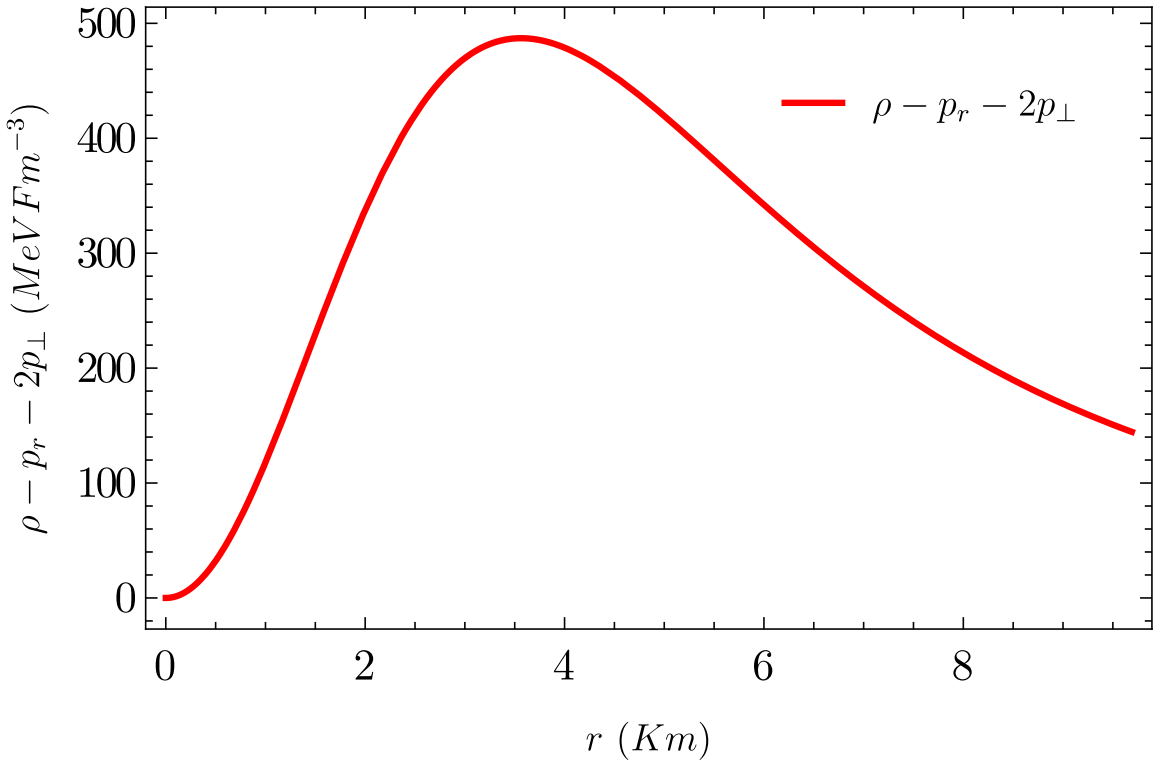

Figure 3.14: Strong energy condition Vs radial variable r.

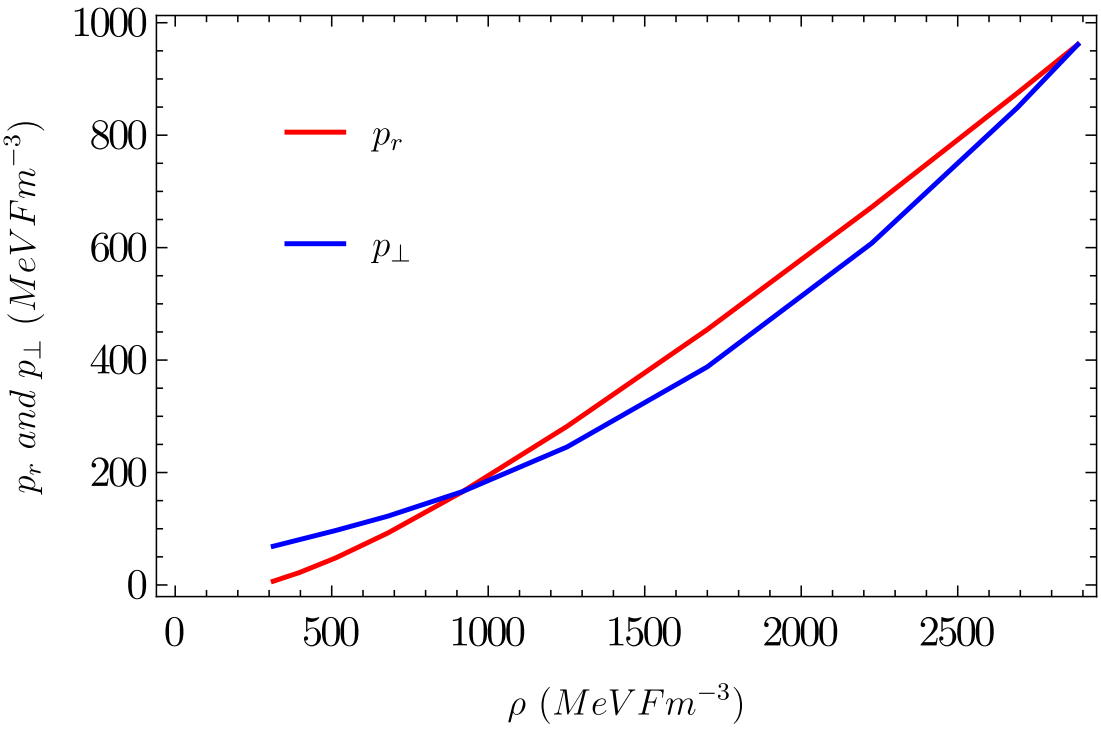

Figure 3.15: Variation of p_r and $p_\perp$ against ρ.

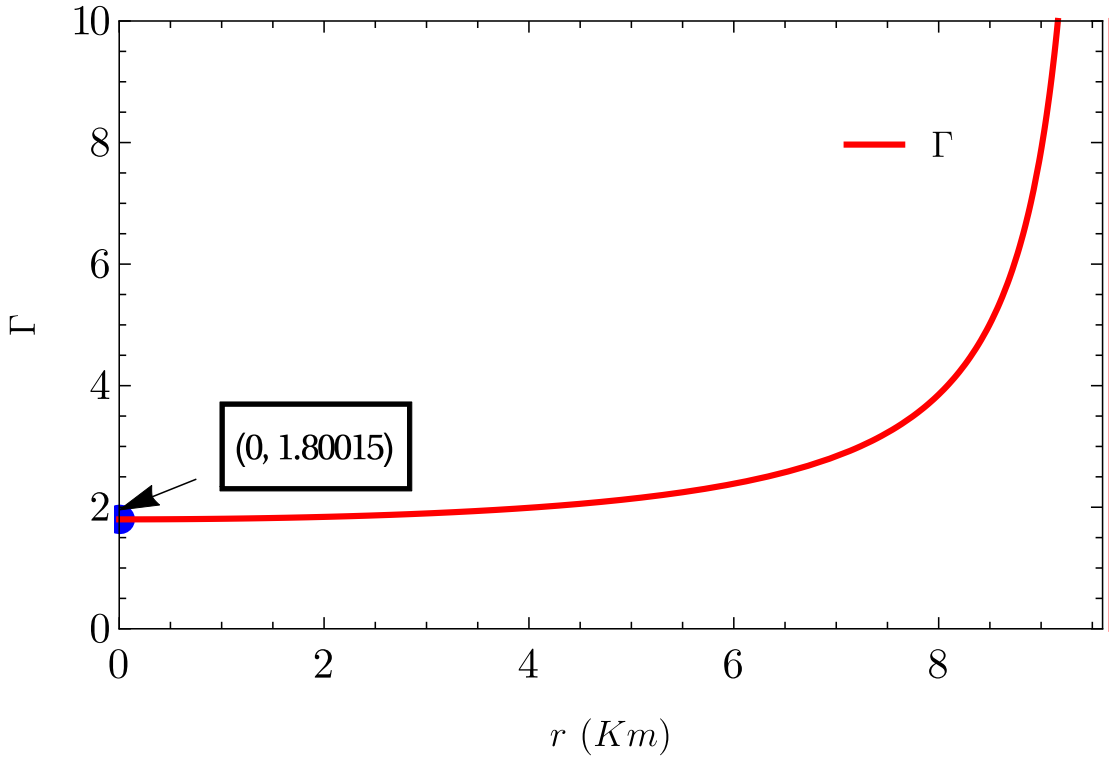

Figure 3.16: Variation of Γ against radial variable r.

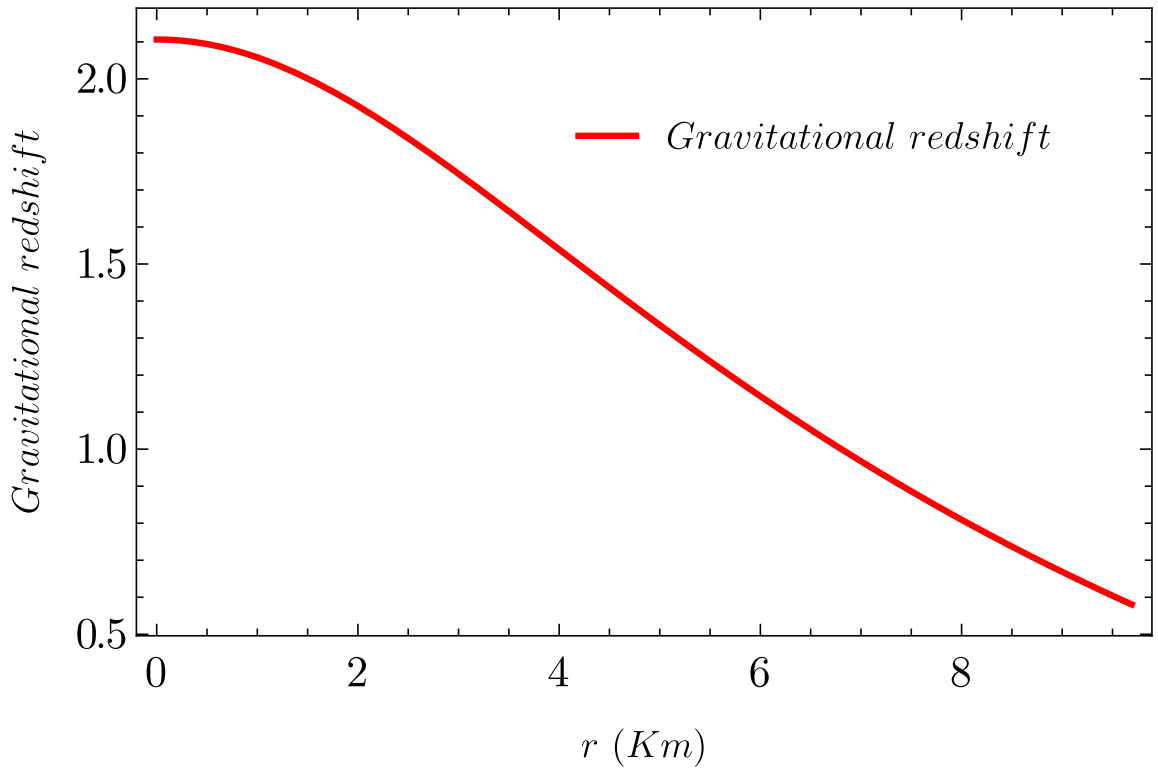

Figure 3.17: Variation of gravitational redshift against radial variable r.